

Research article

Electric and dielectric properties of Fe₂O₃/Silica nanocomposites

S. M. Reda*

Chemistry Department, Faculty of Science, Benha University, Benha, Egypt

*Present address: Chemistry Department, College of Science for girls, Dammam University, Dammam, Kingdom of Saudi Arabia.

E-mail address: safenazr@yahoo.com

Abstract

The Fe₂O₃/SiO₂ nanocomposites have been successfully prepared by sol-gel method using ferric chloride and tetraethylorthosilicate (TEOS) as precursors. The (10:90) Fe₂O₃:SiO₂ molar ratio was prepared at 100 °C and 500 °C. The samples were examined by X-ray powder diffraction (XRD), FT-IR, UV-vis spectroscopy. The results confirmed that the increase of annealing temperature increase the aggregation of Fe₂O₃ nanoparticles and transformed from amorphous to the γ-Fe₂O₃ crystalline state. The optical measurements showed that the particle size of Fe₂O₃ prepared at 100 and 500 °C was 10 and 18 nm, respectively. The effect of increasing temperature on the electric and dielectric properties was analyzed. The results showed that the nanocomposite prepared at 500 °C has the highest conductivity value and dielectric constant. This explained according to particle size effect. **Copyright © IJNST, all rights reserved.**

Keywords: Fe₂O₃/SiO₂ nanocomposite, AC-electrical conductivity, Dielectric Constant, Dielectric loss.

1. Introduction

Organic–inorganic hybrids, or nanocomposites, have proved to be new advanced materials because they combine the advantages of organic components (e.g., flexibility, low dielectric constant (ϵ), and processability) and inorganic components (e.g., rigidity, durability, and thermal stability) [1–5]. Nanocomposite materials with magnetic particles are of great interest due to their various applications [6]. Iron oxides are important materials for many industrial applications such as pigments, magnetic materials, catalysts and sensors [7]. Electrical and magnetic properties of ferrites are strongly dependent on the chemical composition, cation distribution, and method of preparation [7]. Ferrites nanoparticles can be prepared via dry processes (sputtering and CVD) or by liquid-based processes (sol–gel method) [8]. Sol–gel method has been recognized as one of the major materials processing technology in the recent years due to its versatility in synthesizing new materials for a variety of applications. Silicate glass structure has substantial amount of void space within its nanometer sized particles can be accommodated in these glasses. The sol–gel process consists of hydrolysis and condensation reactions [9]. It has several advantages; such as low cost, no special instruments are required [9], fine particles such as ferric salts can be easily and homogeneously mixed with the precursor of silica at the beginning of the experiment. Moreover the possibility to control the properties of the resulting Fe₂O₃ by adjusting different parameters such as, sol concentration, spin speed and annealing temperature [6].

In this paper, we have reported preparation of Fe₂O₃/SiO₂ nanocomposite by sol-gel technique obtained starting from tetraethylorthosilicate (TEOS) and iron chloride hexahydrate FeCl₃ · 6H₂O precursors. The effect of

annealing temperature on electric and dielectric properties of this sample has been investigated to determine the key factors controlling performance of electrical properties.

2. Experimental

2.1. Preparation of Fe₂O₃/SiO₂ nanocomposite powder

The acid-catalyzed sol-gel synthesis was used to prepare iron oxide dispersed in silica matrix. Sol-gel process was carried out under acidic conditions, at pH < 2, in order to prevent the precipitation of the iron hydroxides [8]. Silica precursor sol was prepared by the hydrolysis-condensation reaction of mixing a solution of tetraethoxysilane, Si(OC₂H₅)₄ (TEOS), C₂H₅OH, H₂O and HCl. The TEOS (Fluka), ethanol, H₂O, HCl used for the preparation of silica precursor sol had the molar ratio at 1:1:1.2: 0.1. The sols were prepared by mixing an alcoholic solution of TEOS and aqueous solutions of iron chloride FeCl₃.6H₂O (Aldrich) at 60°C under magnetic stirring for 3 hours. The obtained Xerogel was dried at 100 °C (sample A) and at 500 °C (sample B) for 60 min at each temperature. Scheme 1 shows the steps for preparation of nanocomposites.

2.2 Characterization

A detailed study of the fundamental characteristics of the nanocomposites was conducted by several techniques: (1) X-ray powder diffractometer (Diano Corporation USA diffractometer) with a monochromated Co radiation ($\lambda = 0.179$ nm) was employed to assess the crystallinity of the nanocomposites at room temperature.

(2) The chemical species and the chemical bonding state at different processing parameters were studied employing FTIR spectroscopy (Nicolet spectrometer model 670 FT-IR) in the wave number range 400–4000 cm⁻¹ using KBr pellet.

(3) UV–vis absorption spectra of the nanocomposites were obtained with a Perkin Elmer Lambda 40 spectrophotometer over the spectra range from 200-800 nm.

2.3 Measurements of electrical properties

2.3.1 Electrical conductivity

Measurement of AC-electrical conductivity, σ_{AC} , and its variation with temperature was carried out using a LCR electrometer (PM636 Philips) over a temperature range 303–473K and at frequencies of 1-10³ kHz. The samples of 0.11 cm in thickness and 1 cm in diameter were employed for this study. The specimens were painted with conducting silver paint for providing good electrical contact and were clamped firmly between the electrodes for measurement.

2.3.2 Dielectric measurements

The capacitance (C) and loss factor (D) was measured using LCR electrometer (PM636 Philips) over a temperature range 303–473K and at frequencies of 1-10³ kHz. The test specimens used for the determination of dielectric constant (ϵ') and dielectric loss (ϵ'') were in the form of discs of thickness 0.11 cm and diameter of 1 cm. The specimens were painted with conducting silver paint for providing good electrical contact and were clamped firmly between the electrodes. The arrangement was found to provide good ohmic contact between the sample and the electrodes. The dielectric constant was calculated from the following expression [10]:

$$\epsilon' = \frac{hC}{A\epsilon^o} \quad (1)$$

where h is the thickness of the disc, A the contact area between the sample and the electrode, ϵ^o the permittivity of the free space (8.85×10^{-12} F/m) and C is the capacitance obtained at each frequency.

3. Results and Discussion

3.1 Characterization

X-ray diffraction pattern of the sol-gel-synthesized Fe₂O₃ nanocomposites are shown in Fig. 1. Fig. (1a) shows the amorphous state of sample A. In the case of sample B, the XRD spectra shows characteristic diffraction lines of γ -Fe₂O₃ (maghemite phase) and it seems to be the only phase evidenced by XRD, Fig.(1b). This was attributed to the stabilizing effect of silica matrix [11]. When temperature increases, the confinement effects of the SiO₂ network are weakened, and the Fe₂O₃ crystallites continue to grow. The results are in accordance with that reported by literature [12]. The broad band between $2\theta = 23-27^\circ$ which appears in all XRD pattern is due to amorphous nature of the silica matrix [12].

The crystal size of γ -Fe₂O₃ determined from XRD spectra using the Scherrer formula [11]:

$$D = \frac{0.94\lambda}{\beta \cos \theta} \quad (2)$$

where D is the crystal size of γ -Fe₂O₃, λ the wavelength of X-ray (0.179 nm), θ half diffraction angle of peak (in degree) and β the true half peak width. The average size of the γ -Fe₂O₃ determine through the (311) plane is 20 nm.

Fig. 2 shows the IR spectra of the Fe₂O₃/silica nanocomposites powder. As shown in this Figure the two broad bands at 3435 and 1629 cm⁻¹ are ascribed to the stretching modes and H-O-H bending vibration of the free or absorbed water. Strong absorptions at 1098, 791, 465 cm⁻¹ indicate the formation of silica network [13]. It cannot be observed any characteristic bands of Fe-O-Si bonds. This indicates that there is no interaction between Fe₂O₃ and silica matrix [12]. For B sample Fig. (2b), the intensities for the broad bands associated with the free or absorbed water were drastically weakened. The peak situated at 960 cm⁻¹, due to Si-OH stretching of silanol terminal groups disappears, indicating the progress of the polycondensation process as a consequence of thermal treatment [12]. Also, the band at 1098 cm⁻¹ for Si-O-Si of the SiO₄ tetrahedron and the band at 465 cm⁻¹ associated with Si-O-Si or O-Si-O bending mode grew stronger. These data show that there was a rearrangement process for the silica matrix network with increasing temperature. On the other hand, the Fe-O stretching band in Fe-O-Si bands at 560 cm⁻¹ increases in intensity, which was probably due to the formation of large Fe₂O₃ clusters at higher temperature.

Optical absorption spectra for Fe₂O₃/SiO₂ nanocomposites powder in the UV-vis region are shown in Fig. 3. The Fe₂O₃ showed sharp ultraviolet absorption edges at approximately 377 nm Fig. (3a). The absorption spectrum of sample B shifted to longer wavelengths, 400 nm, suggesting a decrease in the band gap, Fig. (3b). The observed red shift was associated with the growth of cluster dimensions at higher temperature. In a molecular picture, this band gap transition can be considered as being a charge transfer transition from the valence band of Fe₂O₃ and the empty conduction band formed by Fe⁺³ expected to decrease as the number of the interaction valence orbital at oxide and Fe⁺³ increases, i.e. in growing Fe₂O₃ particles. Hence, at lower temperatures, localized transition typical for small iron oxide clusters were observed, while at higher treatment temperature larger clusters were formed thus behaving as bulk Fe₂O₃ [12].

The optical band gap values of Fe₂O₃ nanoparticles dispersed in silica matrix was estimated by plotting $(\alpha h\nu)^n$ as a function of photon energy (hν) using the relation [14]:

$$\alpha h\nu = A(h\nu - E_g)^{\frac{1}{n}} \quad (3)$$

where α is the absorption coefficient, hν is the photon energy and E_g is the optical band gap energy and A is a constant. The linear intercept at the hν-axis gives the value of the band gap. For different values of n, a good linearity was observed at n=4 (indirect allowed transition) for Fe₂O₃, Fig. 4. The band gap values determine for A and B samples were 1.9 and 1.8 eV, respectively. The slight decrease of the band gap energy of B may be due to the increase of the particle size of Fe₂O₃ by increasing temperature. These results were compatible with previsions of the optical band gap for these samples present in literature [15].

According to the Brus model [16], which correlates the optical absorption onset with particle size, the observed spectra are representative for Fe₂O₃ nanocompsites annealed at 100 and 500 °C showing an average diameter of approximately 10 nm and 18 nm, respectively. The increase in particle size by increasing temperature may be due rearrangement of silica matrix network with increasing temperature, which lead to the formation of large Fe₂O₃ clusters at higher temperature. These results are agreed well with the results obtained from the X-ray studies.

3.2 Electrical conductivity

The variation of electrical conductivity, σ_{AC} , with temperature and frequencies was determined for the samples A and B, and is shown in Fig. 5 (a–b). For all samples the σ_{AC} increase with the increasing of the measurement temperature, characteristic of a thermally stimulated process, should be attributed to the increase of the charge carrier's energy, with the rise of the temperature. Thus, and assuming the hopping conductivity model [7], the increase of the charge carriers energy makes easier their hopping motion through the glass matrix free energy barriers. Figure (5a) for sample A shows that, σ_{AC} initially increases up to 408K and then it decreases on further heating up to a temperature of 453K. Then, σ_{AC} increases rather slowly with linearly following Arrhenius behavior up to 473K. The initial rise and later decrease in σ_{ac} , in the region 413–453K is due to desorption of

some absorbed water molecules [7]. Figure (5b) for sample B shows that the σ_{AC} does not change much with variation of temperature up to 408K. On further increase in temperature the value of σ_{AC} increases showing a kink at 453K and later a steep increase in σ_{AC} is observed from 453K to 473K. The presence of kink at 453K indicates the possibility of a hydrogen ferrite phase at this temperature and that the hydrogen ferrite phase decomposes to give a purely vacancy ordered γ -Fe₂O₃ which was observed from the X-ray pattern. The observed electrical conductivity results indicate that γ -Fe₂O₃ samples have only Fe³⁺ state in tetrahedral and octahedral positions. This figure shows also that σ_{AC} increases by increasing frequency. The observed conductivity in the lower frequency can be attributed to the weakly localized carriers which drift over large distances. At higher frequency the mean displacement of these carriers is reduced to show proximity in the conductivity [10].

The temperature dependence of the σ_{AC} , allowing the calculation of activation energy (E_a) using Arrhenius equation [10]:

$$\sigma_{AC} = \sigma_o e^{\frac{-E_a}{2kT}} \quad (4)$$

where k is the Boltzmann's constant and σ_o is the conductivity at infinity temperature. The calculated activation energy for sample A, and B was 0.36 and 0.25 eV, respectively. The higher activation value for sample A may be associated with an increase in the height of the free energy barriers of the quasi-lattice of the glass matrix. Thus, for this electric conductivity behavior, the number of electrical units responsible for the conductivity plays an important role in the decrease of σ_{AC} and increase of E_a for A. The lower values of σ_{AC} , for the A sample, should be assigned to its particles size (10 nm) and particles agglomerates observed in this sample, which leads to a decrease of the free ions number. Hence, it may be understood here that the particle size plays an important role in conductivity.

3.3 Dielectric behavior

The variation of dielectric constant (ϵ') with frequency and temperature for A and B has been shown in Fig. 6 (a–b). It was observed from this figure that the dielectric constant decreases continuously with increase in frequency for all the samples. The decrease in the ϵ' , in all samples, with the increase of the applied field during the heat-treatment, can be associated with an increase in the dipoles number inside the sample. It is observed that, the dielectric constant value for all samples is showing almost a temperature independent behavior. It is understood that the dielectric constant (ϵ') and relaxation frequency are related and depend on temperature [7]. If ϵ' remains unaffected with increase in temperature then relaxation frequency also remains the same, that means that the local carriers are immobile. From Figure 6, it is understood that the local charge carriers are immobile and the thermal activation is negligible. The A sample has lower ϵ' than B sample. The dielectric properties of ferrites are dependent upon several factors; including the method of preparation, chemical composition, grain structure and particle size [7]. The observed dielectric behavior of our samples may be due to the particle size effect [7]. The increase in the particles size for the B sample, verified by the optical measurement, must give origin to a reduction of the electrical dipoles inside the sample and a consequent decreasing of ϵ' . This further suggests that the sample B possesses a high chemical homogeneity and fine grain distribution. This is a normal behavior for high density, fine chemically homogeneous ferrimagnetic material [7].

Figure 7(a-b) shows the variation of dielectric loss with temperature and frequencies for our samples. The loss factor increases from A to B sample indicating a progressive difficulty of the electrical units, inside the sample, in following the applied AC field, with the increase of the out of phase component (ϵ''). The increase of the ϵ'' is due to a diminution of the AC resistivity. This behavior can be ascribed to the increase in the particle size and the diminishing of the electrical carriers inside the material.

4. Conclusion

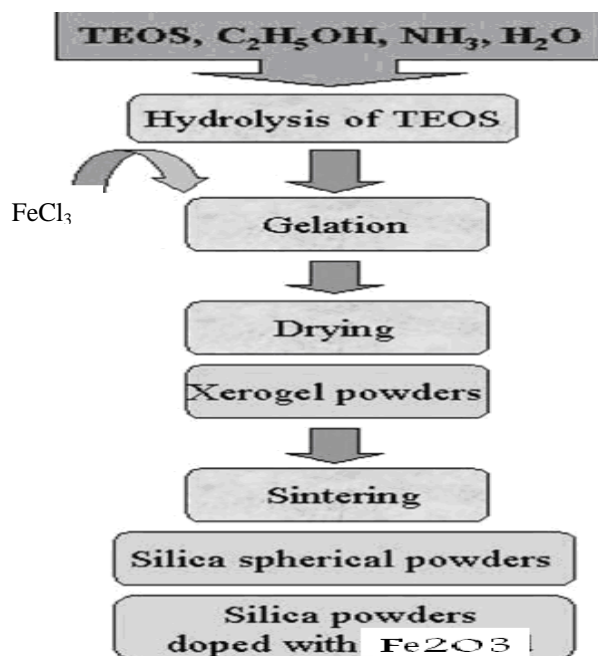
The Fe₂O₃/SiO₂ nanoscale particle size has been prepared via the sol–gel method at different annealing temperatures. At elevated temperatures 500 °C the stable γ -Fe₂O₃ phase development is favored with higher particle size. This indicates that, the higher annealing temperature leading to the frequent particles agglomeration. AC conductivity and dielectric properties were measured at various temperatures and frequencies. The results indicate that AC conductivity and dielectric loss of both composites increased gradually with the increase annealing temperature, due to increase in particle size.

Acknowledgements

The author is greatly acknowledging the physics department, national research center for cooperation and support.

References

- [1] Y. Chen and OI. Jude, Synthesis and characterization of polyimide/ silica hybrid composites, *Chem. Mater.* 11(1999) 1218–1222.
- [2] C. Guizard, A. Bac, M. Barboiu and N. Hovnanian, Hybrid organic- inorganic membranes with specific transport properties: applications in separation and sensors technologies, *Sep. Purif. Technol.* 25 (2001) 167–180.
- [3] J.T.L. Christine, K.C. Bradley and A.W. Jeffrey, In situ polymerization of tetraethoxysilane in polymers: chemical nature of the interactions, *Polymer.* 33 (1992) 1496–1506.
- [4] M. N. Bruce, A. David and V. Celine, Low-density organic-inorganic composite materials via supercritical drying techniques, *Chem. Mater.* 6 (1994) 282–286.
- [5] W. D. Liu, B. K. Zhu, J. Zhang and YY. Xu, Preparation and dielectric properties of polyimide/silica nanocomposite films prepared from sol–gel and blending process, *Polym. Adv. Technol.* 18(2007)522-528.
- [6] R. Kornak, K. Maruszewski, W. Strek, K. Haimanna, W. Dudziński, A. A. Vogt and H. A. Kołodziej, Electric and magnetic properties of sol–gel silica powders doped with ferrofluid, *Journal of Alloys and Compounds.* 380 (2004) 268–273.
- [7] V. A. Hiremath and A. Venkataraman, Dielectric, electrical and infrared studies of γ -Fe₂O₃ prepared by combustion method, *Bull. Mater. Sci.* 26 (2003) 391–396.
- [8] H.C. Caizer, C. Savii and M. Popovici, Magnetic and structural properties of γ -Fe₂O₃ nanoparticles dispersed in a silica matrix, *Journal of Optoelectronics and Advanced Materials.* 2 (2000) 634-638
- [9] H. Ye, X. Zhang, Y. Zhang, L. Ye, B. Xiao, H. Lv and B. Jiang, Preparation of antireflective coatings with high transmittance and enhanced abrasion-resistance by a base/acid two-step catalyzed sol-gel process, *Solar Energy Materials and Solar Cells.* 95 (2011) 2347-2351.
- [10] S. Das and S. Chaudhuri, Temperature dependent dielectric relaxation and electrical conductivity in single-layer ZnO–Al₂O₃ nanocomposite thin films, *phys. stat. sol. (b)*, 244(2007) 2657–2665.
- [11] S. Kumar and R. Chandra: Temperature dependent studies of CdS nanoparticles in viscous matrix. *Optical Materials.* 27 (2005) 1346.
- [12] C. Savii, M. Popovici, C. Enache, J. Subrt, D. Niznansky, S. Bakardzieva, C. Caizer and I. Hriance, Fe₂O₃-SiO₂ composites obtained by sol-gel, *Solid State Ionics.* 15 (2002) 219-227.
- [13] X. Huang and Z. Chen, Nickel ferrite on silica nanocomposites prepared by sol-gel method, *Journal of Magnetism and Magnetic Materials.* 280 (2004) 37-43.
- [14] M. H. Aslan, A. Y. Oral, E. Menşur, A. Gül and E. Başaran, Preparation of c-axis orientation zinc-oxide thin films and the study of their microstructure and optical properties, *Solar Energy Materials and Solar Cells.* 82 (2004) 543-552.
- [15] N. özer and F. Tepehan, Optical and electrochemical characteristics of sol-gel deposited iron oxide films, *Solar Energy Materials and Solar Cells.* 65 (1999) 141-152.
- [16] L. Armelao, M. Fabrizio, S. Gialanella and F. Zordan, Sol-gel synthesis and characterization of ZnO-based nanosystemes, *Thin Solid Films.* 394 (2001)90-96.



Scheme. 1. The steps for preparation of Fe₂O₃/SiO₂ nanocomposite.

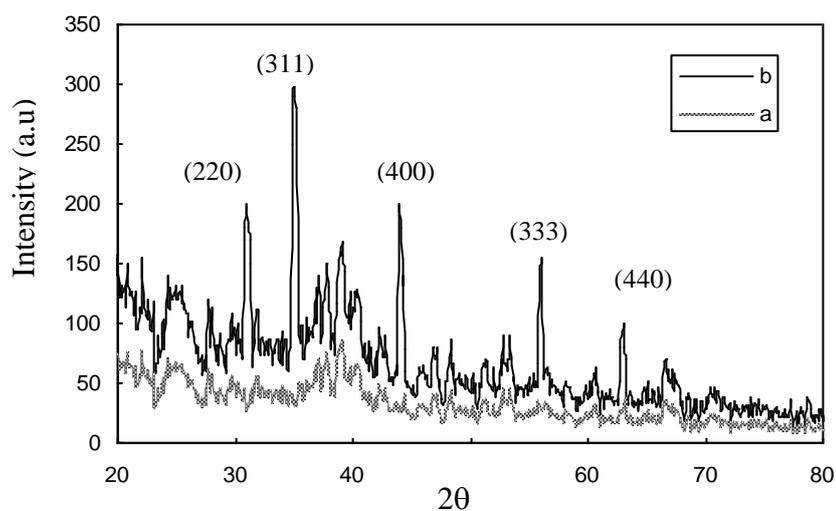


Fig.1. X-ray diffraction patterns of Fe₂O₃ annealed at 100 °C (a) and at 500 °C (b).

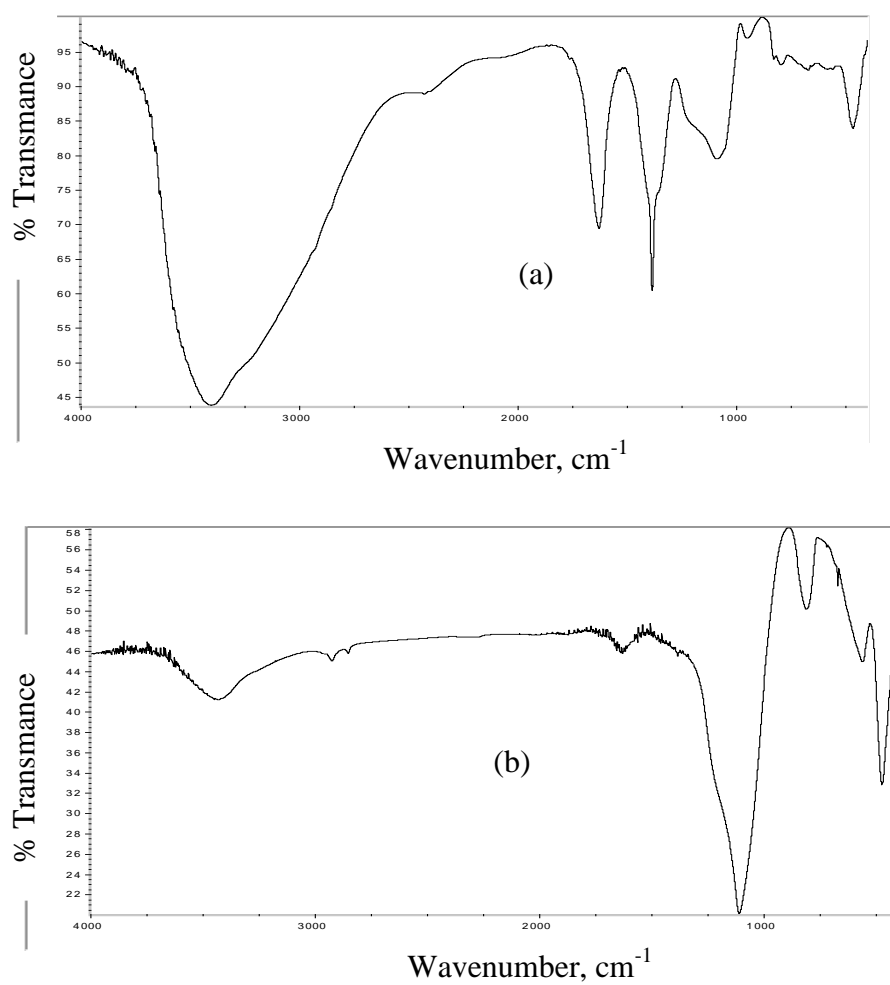


Fig.2. FT-IR spectra of Fe_2O_3 annealed at 100 °C (a) and at 500 °C (b).

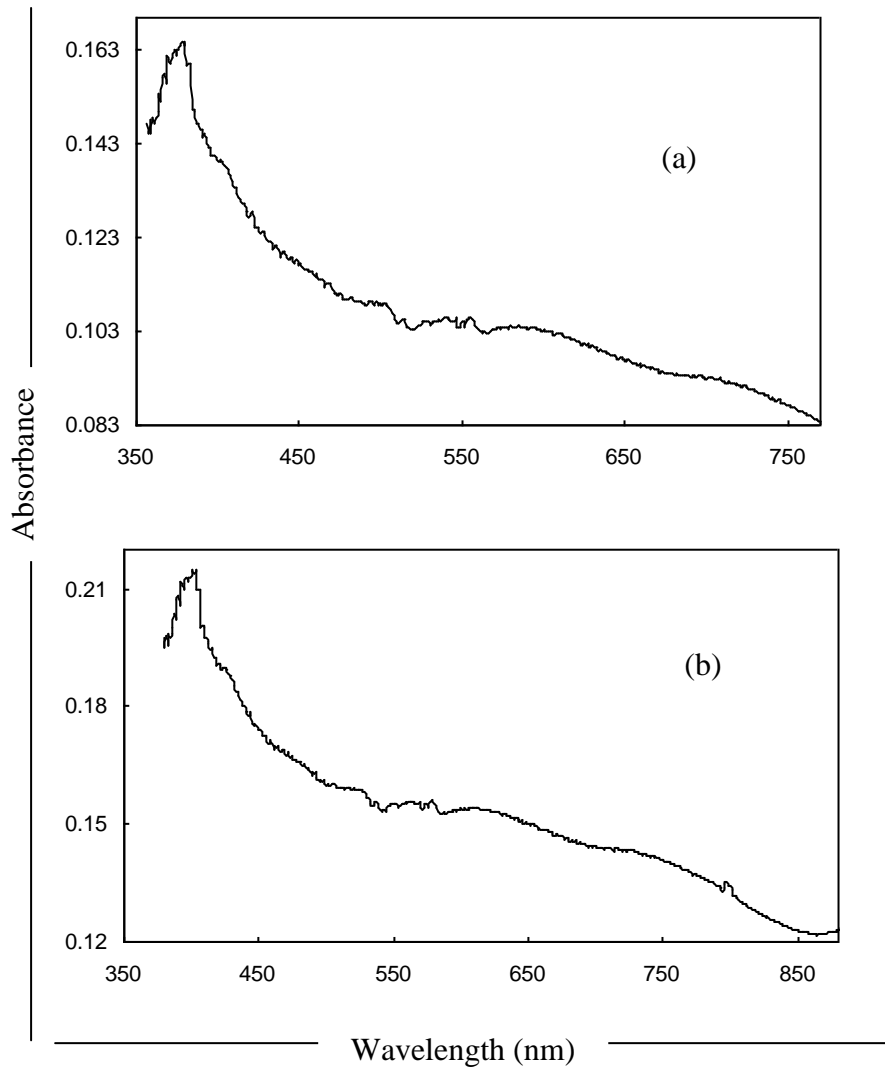


Fig.3. UV-vis optical absorption spectra of Fe₂O₃ annealed at 100 °C (a) and at 500 °C (b).

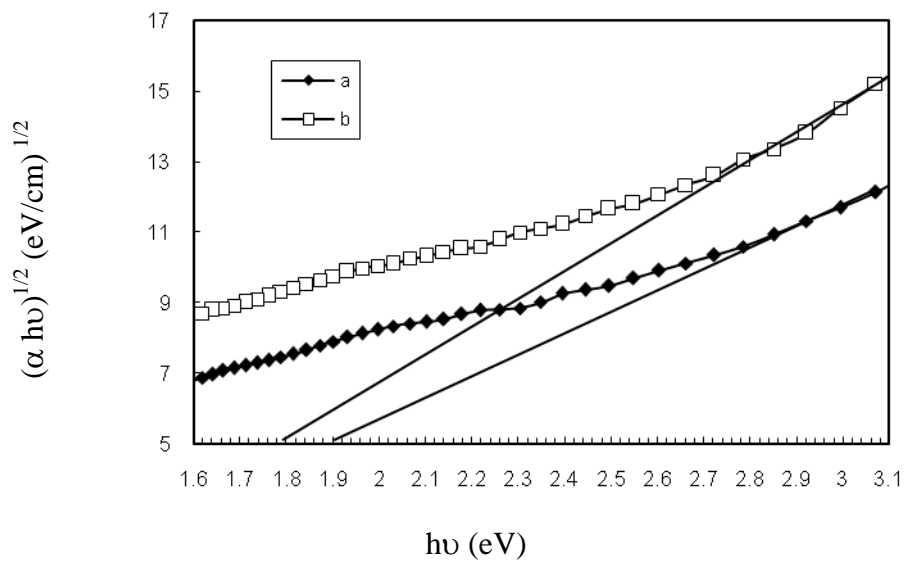


Fig.4. Determination of band gap energy for Fe₂O₃ annealed at 100 °C (a) and at 500 °C (b).

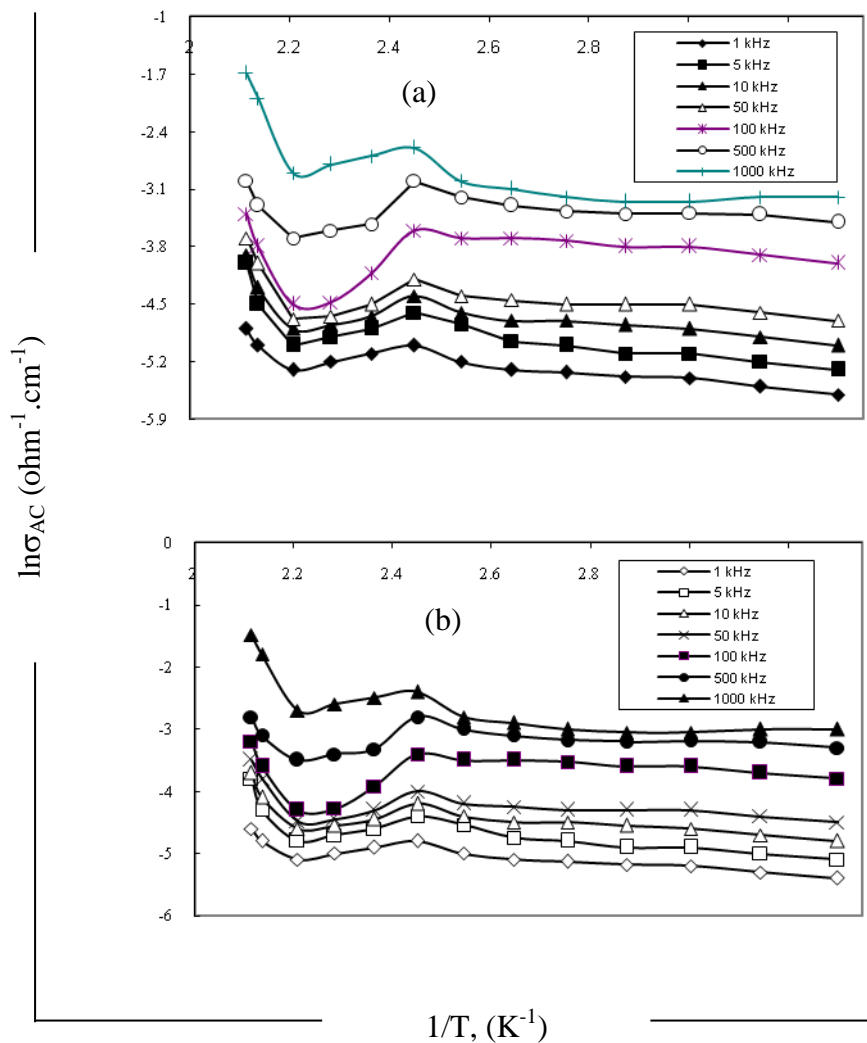


Fig. 5. Effect of temperature on AC-electrical conductivity for Fe₂O₃ annealed at 100 °C (a) and at 500 °C (b).

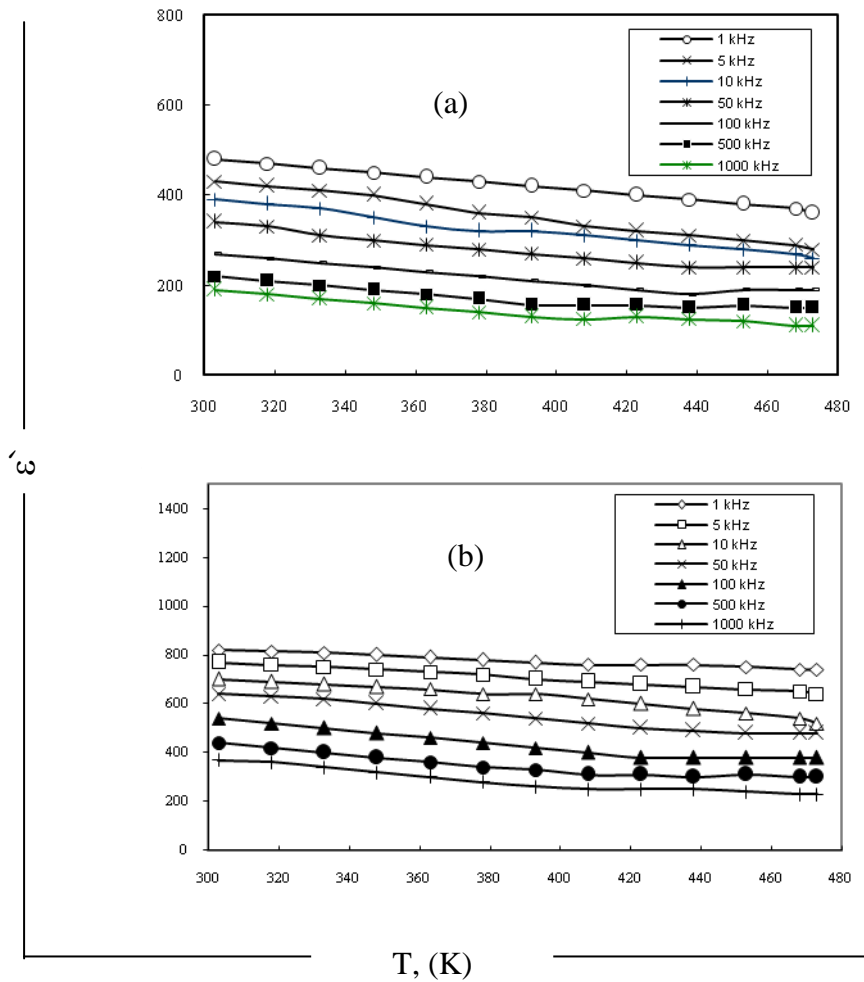


Fig. 6: Effect of temperature on dielectric constant for Fe_2O_3 annealed at 500°C (a) and at 100°C (b).

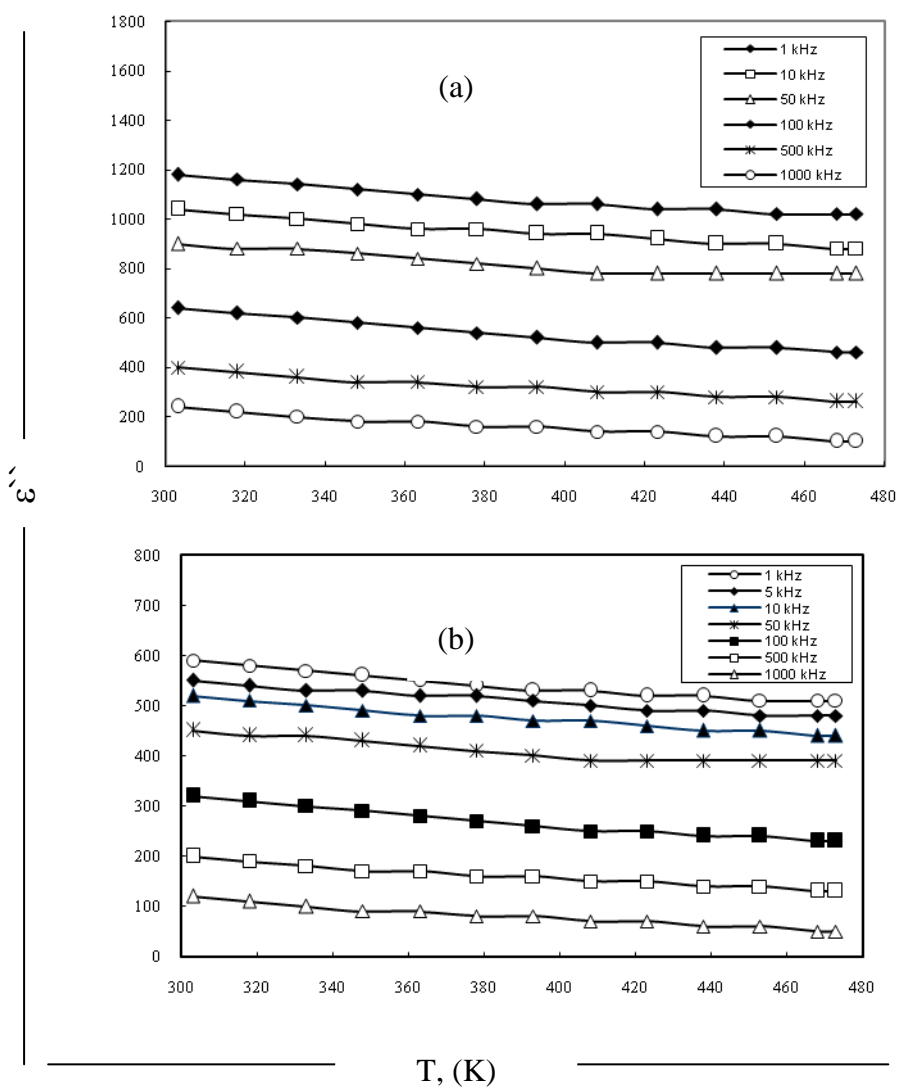


Fig. 7. Effect of temperature on dielectric loss for Fe₂O₃ annealed at 500 °C (a) and at 100 °C (b).